Structural Analysis of Unbonded Concrete Overlays Under Wheel and Environmental Loads

LEV KHAZANOVICH AND ANASTASIOS M. IOANNIDES

At present it is common to treat an overlaid concrete pavement system as a multilayered Kirchhoff plate. A number of finite-element computer programs use this idealization, which assumes that the original slab and the overlay have the same deflection profile, that is, that the two act as an effective, homogeneous plate. Environmental loads, however, are among the most significant factors, making the assumption of equality of the deflection profiles of slab and overlay unacceptable. A formulation proposed by Totsky is implemented into an existing finite-element program to account for the effects of layer separation and compressibility. The effects of combined traffic loading and temperature differentials on the stresses and deflections in the pavement system when the overlay curls away from the existing slab are examined. The product is a finite-element code, abbreviated ILSL2, which represents an extension of the ILLI-SLAB program. Practical illustrative examples of the use of ILSL2 pertaining to typical pavements are presented. When appropriate these results are compared with existing analytical or numerical solutions, including those obtained by using an earlier version of ILLI-SLAB. It was found that both layer compressibility and separation effects need to be accommodated in a reliable mechanistic model for unbonded concrete overlays. If these effects are neglected, significant errors may result.

Structural analysis of portland cement concrete (PCC) overlays is a complex engineering problem. A valid mechanistic model should accommodate the overlaid pavement as a multilayered system subjected to traffic and environmental loads. The model should also take into account pavement joints, which may be mismatched between layers, as well as the possibility of through-the-thickness compression and layer separation. At present it is common to treat a concrete pavement slab overlaid with a PCC or an asphalt concrete overlay as a multilayered Kirchhoff plate. A number of finite-element computer programs use this idealization, which assumes that the original PCC slab and the overlay have the same deflection profile, that is, that the two act as an effective, homogeneous plate.

In a previous paper (*1*) an attempt was made to eliminate one of the plate theory assumptions, namely the requirement of incompressibility for both placed layers (i.e., slab and base or overlay). The authors considered, however, only the case of applied wheel load without environmental loading, such as temperature curling and moisture warping. Environmental loads are among the most significant factors making the assumption of equality of the deflection profiles of slab and overlay unacceptable. This problem has been raised by several investigators (*2,3*). This paper presents a finite-element formulation that accommodates the effects of layer compressibility and the potential for layer separation in concrete pavement systems incorporating two placed layers, for example, slab and overlay or slab and stabilized base. The proposed methodology is well-suited for analysis of partial separation of unbonded PCC overlays.

Department of Civil Engineering, University of Illinois at Urbana-Champaign, 205 North Mathews Avenue, #2230C, Urbana, Ill. 61801.

MECHANICAL MODEL FOR MULTILAYERED CONCRETE PAVEMENTS

The finite-element formulation presented is based on an interesting suggestion first made by Totsky (*4*). This treats a multilayered pavement system resting on a Winkler foundation as a series of alternating plate elements and springs. The plate elements model the bending, whereas the springs accommodate the direct compression occurring in such a system. The contact pressure, q, between two consecutive plates is related to the relative deflection of the two plates, $(\Delta_j - \Delta_{j+1})$, through

$$q = k_I(\Delta_j - \Delta_{j+1}) \tag{1}$$

in which k_I denotes the interlayer spring stiffness.

In the study described here a practical approach has been developed for calculating the interlayer spring stiffness. The following assumptions are made:

1. Compression through the thickness of each placed layer remains independent of the respective bending deformations.
2. Compression of the layers causes only vertical deflections $w(x,y,z)$. Thus, horizontal deflections, $u(x,y,z)$ and $v(x,y,z)$, and therefore horizontal strains, $\epsilon_{xx}(x,y,z)$ and $\epsilon_{yy}(x,y,z)$, are set equal to zero.
3. Vertical strains, $\epsilon_{zz}(x,y)$, are constant (or zero) between any layer surface and the corresponding neutral axis, but they can be different between layers as well as between the upper and lower portions of the same layer. For the case of unbonded PCC overlays it is reasonable to assume in addition that $\epsilon_{zz}(x,y)$ is nonzero only between the two neutral axes.

Denoting the structural characteristics of the upper and lower placed layers by Subscripts 1 and 2, the difference between the vertical deflections of the neutral axis of the upper layer and its bottom surface, $\Delta_1(x,y)$, may be written as

$$\Delta_1(x,y) = \epsilon_{zz1}(x,y)\frac{h_1}{2} = \frac{q(x,y)}{E_1}\frac{(1 - \mu_1 - 2\mu_1^2)}{(1 - \mu_1)}\frac{h_1}{2} \tag{2}$$

where

$\epsilon_{zz1}(x,y)$ = constant value assigned to the vertical strain between the neutral axis of the upper layer and its bottom surface,
$q(x,y)$ = contact pressure arising between the upper and lower layers, and
h_1 = upper layer thickness.

Equation 2 may be rewritten in the form

$$q(x,y) = k_1\Delta_1(x,y) \tag{3}$$

where

$$k_1 = \frac{2E_1(1 - \mu_1)}{h_1(1 - \mu_1 - 2\mu_1^2)} \tag{4}$$

Similarly, for the lower slab

$$q(x,y) = k_2\Delta_2(x,y) \tag{5}$$

where

$$k_2 = \frac{2E_2(1 - \mu_2)}{h_2(1 - \mu_2 - 2\mu_2^2)} \tag{6}$$

and $\Delta_2(x,y)$ is the corresponding difference between the vertical deflections of the neutral axis of the lower layer and its top surface. Accordingly, k_l in Equation 1 can be determined from

$$k_l = \frac{1}{\frac{1}{k_1} + \frac{1}{k_2}} \tag{7}$$

Parameter k_l can be interpreted as an effective stiffness for two springs in series with stiffnesses k_1 and k_2.

This approach for determining k_l can be adapted to accommodate a bituminous interlayer, which is often placed on top of an existing pavement slab before constructing a PCC overlay, for the purpose of providing a leveling course and arresting reflective cracking. Because the eleastic modulus of such a bituminous interlayer, E_b, is much lower than that of either PCC layer, it may be expected that the interlayer will act as a bed of springs whose stiffness, k_b, can be defined as follows:

$$k_b = \frac{2E_b(1 - \mu_b)}{h_b(1 - \mu_b - 2\mu_b^2)} \tag{8}$$

Here h_b and μ_b are the thickness and Poisson's ratio, respectively, for the bituminous interlayer. In this case Parameter k_l in Equation 1 can be considered as an effective stiffness for three springs in series, where

$$k_l = \frac{1}{\frac{1}{k_1} + \frac{1}{k_2} + \frac{1}{k_b}} \tag{9}$$

with k_1 and k_2 given by Equations 4 and 6, respectively.

FINITE-ELEMENT IMPLEMENTATION

Implementation of Totsky's approach in a finite-element code requires the introduction of a special eight-noded (24 degree-of-freedom) element (Figure 1). The first four nodes are placed at the neutral axis of the upper plate, whereas the other four nodes are placed at the neutral axis of the lower plate. The stiffness matrix for this element is

$$[K] = \begin{bmatrix} [K_{PL1}] + [K_{KDI}] & -[K_{DLI}] \\ -[K_{DLI}] & [K_{DLI}] + [K_{PL2}] + [K_{DLS}] \end{bmatrix} \tag{10}$$

where

$[K_{PL1}]$ and $[K_{PL2}]$ = stiffness matrices for the upper and lower plates, respectively;
$[K_{DKI}]$ = stiffness matrix for the interlayer springs; and
$[K_{DLS}]$ = stiffness matrix for the dense liquid (DL) subgrade.

The stiffness matrix in Equation 10 has been incorporated into the library of elements of computer program ILLI-SLAB (1989 version) (*5*). The resulting extended version of the code is abbreviated here as ILSL2. In view of the potential for separation under temperature loading, the proposed formulation in ILSL2 assumes for simplicity that the stiffness matrices for both the spring interlayer and the subgrade are dependent only on nodal deflections and not on modal rotations. The interlayer stiffness k_l may be specified by the user. Alternatively, the program will calculate it from the plate parameters by using Equation 7.

The following iterative scheme is adopted in ILSL2 for analyzing an unbonded three-layer system with applied external and temperature loads.

1. Formulate individually the stiffness matrices for the two plates, the spring interlayer, and the subgrade.
2. Combine these matrices as indicated by Equation 10 to form the global stiffness matrix.
3. Formulate individually the load vectors for the external applied load (upper plate), the self-weight (both plates), and the tem-

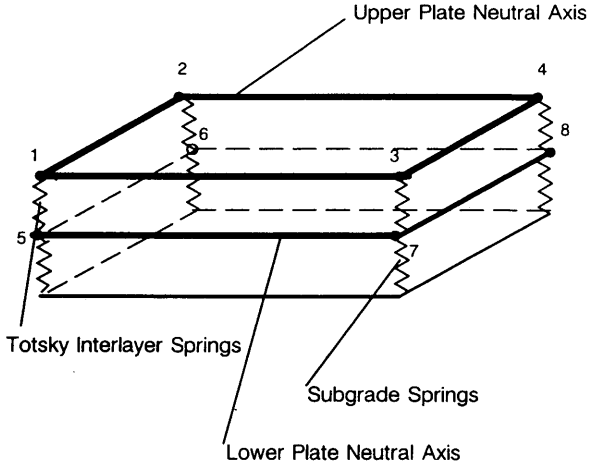

FIGURE 1 Finite-element idealization for two plates with Totsky interlayer springs resting on dense liquid foundation.

perature differentials (both plates) (*6*). In this paper a positive temperature differential, ΔT, indicates that the top surface is warmer than the bottom surface.

4. Combine these load vectors into the corresponding global load vector.

5. Solve the resulting system of equations to determine the nodal deflections and rotations.

6. Check the vertical deflection at each node to determine whether contact is maintained along the two interfaces, that is, between the upper and lower plates and between the lower plate and the subgrade.

7. If the deflection of the lower plate is negative (upward) contact with the subgrade has been lost. Therefore, set the corresponding subgrade spring equal to zero.

8. Similarly, if the difference in deflections at corresponding nodes in the two plates is negative, then the two plates are no longer in contact. In this case set the corresponding interlayer spring equal to zero.

9. Return to Step 1 and perform another iteration, continuing the process until the contact condition at all nodes remains unchanged during two consecutive iterations.

VERIFICATION OF PROPOSED FINITE-ELEMENT FORMULATION

Two series of finite-element runs detailed elsewhere (*7*) have verified that for certain special cases Totsky's approach implemented in ILSL2 gives the same results as the earlier ILLI-SLAB (1989 version) code, as expected. In addition, these runs have shown that for inputs close to these special points ILSL2 solutions are reasonably different and exhibit no abrupt jumps. For example, decreasing the flexural stiffness of the lower placed layer (e.g., the existing slab) leads to a reduction in its influence on the deformation of the upper placed layer (e.g., the overlay slab). In the limit, as the thickness of the lower layer tends to zero, subgrade and interlayer work together as a springs-in-series foundation, whose effective stiffness, k_e, is given by

$$k_e = \frac{1}{\frac{1}{k_I} + \frac{1}{k}} \tag{11}$$

On the other hand, increasing the flexural stiffness of the lower layer results in greater resistance to the bending offered by this layer. Consequently, the deflection profile of the lower layer becomes flatter, and in the limit this layer experiences only a rigid body motion because of the compressibility of the subgrade and the self-weight of the upper layer. At that extreme the lower layer acts like a rigid (no bending) base for the upper layer and the interlayer, and the subgrade adds a constant increment to the deflection of the upper layer at all points.

In addition, ILSL2 runs show that when the interlayer spring stiffness k_I is very high ($k_I \approx 2.71 \times 10^6$ to 2.71×10^8 MPa/m, or 10^7 to 10^9 psi/in.), the bending stresses at the bottom of both the upper and lower layers are practically identical to those calculated by using the earlier version of ILLI-SLAB or using the DL "closed-form" plate theory method proposed by Ioannides et al. (*1*). The latter method employs Westergaard's well-known equation (*8*), into which an equivalent plate thickness is introduced. In all cases the two placed layers were assumed to be unbonded. Such close agreement is to be expected, because very high k_I values denote that neither placed layer experiences compression through its thickness, in accordance with plate theory. It was also observed that as k_I decreases the bending stress in the upper layer increases quite significantly, whereas the corresponding stress in the lower layer decreases, albeit much less dramatically. Both stresses are particularly sensitive to the value of k_I if the latter drops below 2.71×10^5 MPa/m (10^6 psi/in.). The proposed Equation 7 yields a k_I value of 9.97×10^4 MPa/m (3.673×10^5 psi/in.), at which value both stresses are significantly different from those predicted by conventional plate theory applications.

From these observations it can be concluded that Totsky's approach provides a useful enhancement of conventional finite-element analysis of concrete pavements and can be used to account for through-the-thickness compressibility neglected in conventional plate theory applications. Good agreement with available numerical and analytical solutions verifies the robustness of the finite-element formulation introduced in this paper.

PRACTICAL EXAMPLES

To investigate the effects of separation between an existing slab (SL) and its overlay (OL) and of the compressibilities of these two placed pavement layers, a typical airport pavement loaded with a Boeing 727 (B-727) aircraft at the edge or corner was considered. Results are presented in Tables 1 to 3. The thicknesses of SL and OL were 406 mm (16 in.) and 178 mm (7 in.), respectively. The modulus of the subgrade reaction was assumed to be 54 MPa/m (200 psi/in.), whereas the stiffness of the interlayer springs, calculated according to Equation 7, was set equal to 9.97×10^4 MPa/m (3.673×10^5 psi/in.). Linear temperature variations, which could be different through the thicknesses of SL and OL, were also imposed. All pavement system parameters employed are given in Table 1. Several runs were conducted, in which the temperature gradient ($\Delta T_j/h_j$) in the overlay, g_{OL}, and in the existing slab, g_{SL}, was varied. Differences between the results from ILLI-SLAB and ILSL2 were also examined.

Edge Loading

For conventional analysis of airport pavements, edge loading is considered critical. To study this type of loading, a series of nine runs was performed, as shown in Table 1. A rather broad range of temperature gradients was assumed here to highlight temperature loading effects and to permit inferences with respect to the consequences of less severe conditions. Table 1 shows the magnitude of maximum tensile bending stresses arising at the top and bottom of OL and SL, σ_{OL}, σ_{OLb}, σ_{SL}, and σ_{SLb}, respectively. Results obtained indicate that maximum tensile bottom stresses occur under the load, whereas maximum tensile top stresses occur at some radial offset from the load, typically on the order of 1.8 to 2.4 m (6 to 8 ft).

A detailed examination of the stresses in Table 1 can begin with the baseline case of no-curling conditions for both OL and SL (i.e., $g_{OL} = g_{SL} = 0$). For this case a qualitative coincidence of results from ILSL2 and ILLI-SLAB is noted. Both codes show that the maximum tensile top and bottom stresses in SL exceed those in OL. Furthermore, the maximum tensile bottom stresses

TABLE 1 MPa Under Edge Loading with B-727

g_{OL}	g_{SL}	σ_{OLt}		σ_{OLb}		σ_{SLt}		σ_{SLb}	
(°C/cm)		ILSL2	ILLI-SLAB	ILSL2	ILLI-SLAB	ILSL2	ILLI-SLAB	ILSL2	ILLI-SLAB
-0.66	-0.66	1.05	1.05	1.40	0.72	2.41	2.41	1.54	1.66
0.00	-0.66	0.21	0.	2.88	2.32	2.65	1.97	1.33	1.41
+0.66	-0.66	0.72	0.	5.35	3.92	2.96	2.90	1.12	1.17
-0.66	0.00	2.14	2.15	1.29	0.	1.01	1.02	2.87	3.14
0.00	0.00	0.53	0.53	1.98	1.31	1.21	1.21	2.86	2.99
+0.66	0.00	0.21	0.	3.50	2.94	1.41	1.41	2.76	2.84
-0.66	+0.66	3.50	3.47	2.12	0.	0.58	0.13	4.72	5.05
0.00	+0.66	1.94	1.90	1.90	0.42	0.44	0.65	4.59	4.85
+0.66	+0.66	0.32	0.33	2.70	2.03	0.75	0.75	4.52	4.65

Notes: P=2x178 kN; p=1.17 MPa.; L=6 m x 6 m
h_{OL}=178 mm, h_{SL}=406 mm; $E_{OL}=E_{SL}=2.76\times10^4$ MPa; $\mu_{OL}=\mu_{SL}=0.15$;
$\alpha_{OL}=\alpha_{SL}=9\times10^{-6}$ ε/°C; $\gamma_{OL}=\gamma_{SL}=23.6$ kN/m
k=54 MPa/m, $k_I=9.97\times10^4$ MPa/m
Finite Element Mesh: 325 elements (half slab), 21.6 to 25.4 cm on side; Element Aspect Ratio = 1 to 1.2

TABLE 2 MPa Under Edge Loading of Bare Slab with B-727 Using ILSL2

g_U	g_L (°C/cm)	σ_{SLb}	σ_{SLt}
-0.66	0.00	4.30	0.048
0.00	0.00	3.20	0.400
+0.66	0.00	2.21	0.765

Notes: All parameters same as in Table 1, except h_{OL}=0. The 406-mm SL is analyzed as two bonded plates, 178 mm and 228 mm thick, respectively. No interface springs are used.

TABLE 3 MPa Under Corner Loading with B-727

g_{OL}	g_{SL}	σ_{OLt}		σ_{OLb}		σ_{SLt}		σ_{SLb}	
(°C/cm)		ILSL2	ILLI-SLAB	ILSL2	ILLI-SLAB	ILSL2	ILLI-SLAB	ILSL2	ILLI-SLAB
-0.66	-0.66	1.47	1.48	1.43	0.88	3.36	3.36	1.90	2.01
0.00	-0.66	0.32	0.	2.94	2.45	3.59	3.61	1.62	1.70
+0.66	-0.66	1.01	0.	5.63	4.02	3.80	3.86	1.15	1.40
-0.66	0.00	2.73	2.72	0.94	0.	2.32	2.31	2.19	2.36
0.00	0.00	1.11	1.11	1.48	0.92	2.53	2.53	1.99	2.09
+0.66	0.00	0.28	0.	3.02	2.50	2.71	2.76	1.72	1.81
-0.66	+0.66	4.16	3.96	1.83	0.	1.24	1.26	2.32	2.77
0.00	+0.66	2.50	2.37	0.88	0.	1.53	1.53	2.28	2.46
+0.66	+0.66	0.86	0.79	1.54	0.94	1.80	1.79	2.05	2.15

Notes: All pavement system parameters same as in Table 1.
Finite Element Mesh: 325 elements (full slab), 19.5 to 76.2 cm on side; Element Aspect Ratio = 1 to 3.9

are higher than those at the top for both SL and OL. As was also the case for interior loading, however, Totsky's approach in ILSL2 results in a significantly higher σ_{OL_b} than the conventional approach in ILLI-SLAB (1.98 cf. 1.31 MPa, or 287 cf. 190 psi).

To investigate the cause for this difference an additional no-curling run with ILSL2 was conducted in which the interface spring stiffness k_i was set to a very high value (2.71×10^7 MPa/m, or 10^8 psi/in.). Thus, SL and OL were assumed to be free to separate but not to possess any compressibility. A value of σ_{OL_b} = 1.42 MPa (206 psi) was obtained in this case, indicating that layer separation is responsible for only one-sixth of the increase predicted by ILSL2, the bulk of this change being attributable to layer compressibility. It is therefore imperative to account for compressibility in the analysis and design of unbonded concrete overlays.

Consider next the two cases with g_{SL} equal to 0 and g_{OL} varying, which are also very important from a practical point of view. Field measurements suggest that daily cycle temperature changes result in a high temperature gradient near the top surface of a concrete pavement and that the value of this gradient decreases with depth (*9,10*). Table 1 shows that as g_{OL} changes from −0.66 to +0.66°C/cm (−3 to +3°F/in.) a significant increase in σ_{OL_b} is observed, whereas σ_{OL_t} decreases considerably. Indeed, for g_{OL} equal to +0.6°C/cm (+3°F/in.), σ_{OL_b} from ILSL2 is almost twice the corresponding value obtained for no-curling conditions (3.50 cf. 1.98 MPa, or 507 cf. 287 psi). The difference in σ_{OL_t} is even more dramatic: decreasing g_{OL} from 0 to −0.66°C/cm (0 to −3°F/in.) causes a fourfold increase in σ_{OL_t} predicted by ILSL2 (from 0.53 to 2.14 MPa, or from 77 to 311 psi). Similar comparisons can be made by using results from ILLI-SLAB.

It is therefore apparent that as far as OL is concerned, critical stress conditions (i.e., overall maximum values of bending stress for the three g_{OL} values considered) arise at the bottom when a positive g_{OL} is introduced (3.50 MPa or 507 psi), whereas a negative g_{OL} causes a critical stress at the top (2.14 MPa, or 311 psi). Although for these three cases critical stress at the bottom of OL is higher than that at the top (3.50 cf. 2.14 MPa, or 507 cf. 3311 psi), the latter is still appreciable and should not be disregarded. Recall that the upper portion of OL is more susceptible to freeze thaw or other environmental damage and may therefore be more prone to rapid crack propagation, even at moderate stress levels.

By comparison stresses in SL are influenced to a much lesser degree by changes in g_{OL}. Critical stress arises at the bottom of SL for a negative g_{OL} (2.87 MPa or 416 psi), and at the top of SL for a positive g_{OL} (1.41 MPa or 204 psi). The larger of these two stresses is practically the same as that for no-curling conditions (2.87 cf. 2.86 MPa, or 416 cf. 415 psi). In fact, it is important to note that for the three cases considered here this value is about 20 percent smaller than the overall maximum stress in OL (2.87 cf. 3.50 MPa, or 416 cf. 507 psi). This observation suggests that under temperature loading it is inappropriate to assume that stresses in SL will always be higher than those in OL. This is only the case in the absence of curling, when it can be attributed directly to the lower flexural stiffness of OL. A fairly thin unbonded overlay may still be subjected to excessive stresses. This justifies the 150-mm (6-in.) minimum thickness recommended by the Portland Cement Association for such overlays (*11*).

The remaining six cases in Table 1 examine the influence of several combinations of temperature gradients in SL and OL. It is again observed that stresses in SL are considerably more sensitive to changes in g_{SL} than to changes in g_{OL}. This does not imply, however, that the response of SL is unaffected by the presence of OL. Under field conditions the thermal properties of OL may influence the development of g_{SL} considerably by slowing down any cooling and warming in SL. For example, in the early afternoon, OL will provide thermal insulation for SL, thus preventing g_{SL} from rising to high positive values. This will reduce the probability of high stresses at the bottom of SL. Consequently, the ILSL2 prediction for σ_{SL_b} for g_{OL} equal to 0.66°C/cm (+3°F/in.) and g_{SL} equal to +0.22°C/cm (+1°F/in.) would be only 3.43 MPa (498 psi), compared with a value of 4.52 MPa (656 psi) for g_{OL} equal to g_{SL} equal to +0.66°C/cm (+3°F/in.) given in Table 1. Additional comments with regard to this important thermal blanket function of unbonded overlays are made in a subsequent paragraph.

On the other hand, OL stresses are sensitive to changes in both gradients. A worst-case scenario arises when the external load is combined with gradients of opposite signs in SL and OL. The combination of a negative g_{OL} with a positive g_{SL} is critical for SL, whereas for OL the critical pair is a positive g_{OL} and a negative g_{SL}. Both extremes occur at the respective bottom surfaces. These trends may have been expected, because under these environmental conditions separation between OL and SL, as well as between SL and subgrade, is most pronounced.

It is also observed that the conventional approach in ILLI-SLAB may significantly underestimate stresses in OL [e.g., σ_{OL_b} = 3.92 cf. 5.35 MPa (568 cf. 776 psi), for g_{OL} = +0.66°C/cm (+3°F/in.) and g_{SL} = −0.66°C/cm (−3°F/in.)]. In several cases ILLI-SLAB predicts that the entire top or bottom surface of OL experiences only compression (the entry in Table 1 is zero). In contrast, ILSL2 indicates the presence of significant tensile stresses as well. Such results underscore the effects of separation and compressibility introduced in ILSL2. On the other hand, ILLI-SLAB predictions for both the top and bottom of SL are reasonably close to those from ILSL2, being slightly higher for σ_{SL_b} and slightly lower for σ_{SL_t}. For typical PCC pavements, in which the flexural stiffness of SL exceeds that of OL, the response of SL will be largely insensitive to separation and compressibility effects.

The thermal blanket effect of unbonded PCC overlays identified above deserves some additional exploration. Conventional analysis usually suggests that the effectiveness of such overlays in reducing the bending stresses in the existing slab is severely limited. Three additional finite-element runs were conducted to reexamine this assertion, as shown in Table 2. In these runs the same existing slab was considered as in Table 1, but without the overlay. The 406-mm (16-in.) SL is subdivided into two bonded plates, 178 mm (7 in.) and 229 mm (9 in.) thick, respectively. Furthermore, the gradient in the lower plate, g_L, is assumed to be zero. Thus, SL responses in Table 2 are comparable to those in Table 1 with g_{SL} equal to 0. The gradient in the upper plate, g_U, was allowed to vary between −0.66 and +0.66°C/cm (−3 and +3°F/in.), as would be the case if the pavements in Tables 1 and 2 were in the same general climatic region. For the case of no curling, Table 2 shows that the maximum tensile stress at the bottom of the slab (lower plate), σ_{SL_b}, is 3.20 MPa (464 psi). This value is only 7 percent higher than 2.99 MPa (434 psi), the stress predicted for the overlaid slab by the conventional approach in ILLI-SLAB (see Table 1). Note that both these stress values ignore compressibility effects. This justifies earlier observations about the small contribution of OL in reducing σ_{SL_b} on the basis of the flexural stiffnesses of the two placed layers alone. When an upright gradient of −0.66°C/cm (−3°F/in.) is considered, however, the bare slab

experiences 4.30 MPa (623 psi), compared with 2.87 MPa (416 psi) in the overlaid slab of Table 1. The latter value is obtained by using the proposed, more realistic ILSL2 model. Therefore, the overlay effectively reduces $\sigma_{SL,b}$ by 50 percent through its impact on g_{SL} (i.e., by preventing a negative gradient in SL). Given the thermal protection that the overlay provides to the slab, the only way to increase $\sigma_{SL,b}$ while maintaining g_{OL} at −0.66°C/cm (−3°F/in.) is to allow g_{SL} to assume a high positive value. Yet even under the extremely severe combination of g_{OL} equal to 0.66°C/cm (−3°F/in.) and g_{SL} equal to +0.66°C/cm (+3°F/in.), Table 1 shows that $\sigma_{SL,b}$ from ILSL2 is 4.72 MPa (684 psi), that is, only 10 percent higher than the bare slab value of 4.30 MPa (623 psi) in Table 2. Thus, the presence of the overlay mitigates significantly what could have been disastrous temperature loading on the bare slab.

It should also be pointed out in Table 2 that for such a thick slab, daytime conditions (g_U = −0.66°C/cm or +3°F/in.) can be less severe (2.21 MPa or 320 psi) than no-curling conditions (3.20 MPa or 464 psi) or nighttime conditions (g_U = −0.66°C/cm or −3°F/in.; 4.30 MPa or 623 psi). This finding is in agreement with earlier investigations into the effect of nonlinear (or bilinear) temperature distributions (*5,9,10*).

Corner Loading

Corner cracking is one of the most common forms of distress exhibited by unbonded concrete overlays. To examine this phenomenon a series of nine runs was performed by using the same pavement system parameters given in Table 1. Results obtained under corner loading indicate that maximum tensile bottom stresses occur under one of the tire prints. Maximum tensile top stress location varies, most frequently occurring at some radial offset from the load, typically on the order of 1.5 to 2 m (5 to 7 ft). The magnitudes of maximum tensile bending stresses arising at the top and bottom of OL and SL, $\sigma_{OL,t}$, $\sigma_{OL,b}$, $\sigma_{SL,t}$, and $\sigma_{SL,b}$, respectively, are shown in Table 3.

For the baseline case of no curling, ILSL2 and ILLI-SLAB results in Table 3 show that maximum tensile top and bottom stresses in SL exceed those in OL, consistent with the relative flexural stiffnesses of SL and OL. Furthermore, $\sigma_{SL,t}$ is higher than $\sigma_{SL,b}$, as expected for corner loading. Yet ILSL2 predicts that $\sigma_{OL,b}$ is higher than $\sigma_{OL,t}$, whereas ILLI-SLAB suggests the reverse. As discussed above for edge loading, the conventional approach in ILLI-SLAB significantly underestimates $\sigma_{OL,b}$ in comparison with Totsky's approach in ILSL2 (0.92 cf. 1.48 MPa, or 133 cf. 215 psi). The primary contributor to this discrepancy is the effect of layer compressibility.

Examination of results obtained for the three cases of g_{SL} equal to 0 and g_{OL} varying reveals that the influence of g_{OL} on maximum tensile stresses is similar to that observed under edge loading. Table 3 demonstrates that as g_{OL} changes from −0.66 to +0.66°C/cm (−3 to +3°F/in.), a significant increase in $\sigma_{OL,b}$ is observed, whereas $\sigma_{OL,t}$ decreases considerably. For g_{OL} equal to +0.66°C/cm (+3°F/in.), $\sigma_{OL,b}$ from ILSL2 is more than twice the value obtained for no-curling conditions (3.02 cf. 1.48 MPa, or 438 cf. 215 psi). For g_{OL} equal to +0.66°C/cm (−3°F/in.), the same is true for $\sigma_{OL,t}$ (2.73 cf. 1.11 MPa, or 396 cf. 161 psi). These trends suggest that conclusions reached for edge loading are valid for corner loading as well. Critical OL stress conditions (i.e., overall maximum values of bending stress for the three g_{OL} values considered) occur at the bottom when a positive g_{OL} is acting, whereas a negative g_{OL} may produce a critical stress at the top. Comparing corresponding cases in Tables 1 and 3 for g_{SL} equal to 0 shows that $\sigma_{OL,b}$ is higher under edge loading, whereas corner loading causes a higher $\sigma_{OL,t}$. As mentioned earlier, even a moderate level of top stresses in OL can cause significant damage. Therefore, it can be concluded that corner loading may be critical under conditions of severe negative g_{OL}, leading to considerable OL cracking.

The remainder of the cases in Table 3 illustrate the effect of several combinations of temperature gradients in SL and OL. It is again observed that stresses in SL are considerably more sensitive to changes in g_{SL} than to changes in g_{OL} and that OL stresses are sensitive to changes in both gradients. As might have been anticipated following the discussion of Table 1, critical conditions arise when the external load is combined with gradients of opposite signs in SL and OL. Under corner loading the combination of a positive g_{OL} with a negative g_{SL} is critical for SL, with the overall maximum stress occurring at the top.

As far as OL is concerned, the combination of a positive g_{OL} with a negative g_{SL} is critical under corner loading, just as it was for edge loading. Under these conditions, $\sigma_{OL,b}$ from ILSL2 is 5.63 MPa (817 psi), the overall highest stress among all cases considered, including those for edge loading. This high level of stress can be attributed to widespread separation between OL and SL. This assertion may be verified by reanalyzing this case by using ILSL2 with k_l set to a very high value [e.g., 2.71×10^7 MPa/m (10^8 psi/in.)]. In contrast, ILLI-SLAB predicts a significantly lower value for $\sigma_{OL,b}$ (4.02 MPa or 583 psi). The combination of a negative g_{OL} with a positive g_{SL} leads to critical $\sigma_{OL,t}$ (4.16 MPa or 604 psi), but this stress is smaller than the $\sigma_{OL,b}$ quoted above. Top OL stress predictions from both ILSL2 and ILLI-SLAB are comparable for this temperature gradient combination. This suggests that neither layer separation nor compressibility has much influence on critical bending stresses in this case, contrary perhaps to intuitive expectations.

Stress and Deflection Profiles

Examination of critical bending stresses in the preceding paragraphs revealed that layer compressibility and separation effects can be quite significant in a number of cases. On the other hand, agreement between ILSL2 and ILLI-SLAB in several cases was quite good, even surprisingly so. Consider, for example, the case of corner loading with g_{OL} equal to −0.66°C/cm (−3°F/in.) and g_{SL} equal to +0.66°C/cm (+3°F/in.), for which the $\sigma_{OL,t}$ values predicted by ILLI-SLAB and ILSL2 were 3.96 and 4.16 MPa (574 and 604 psi), respectively. For this case it would have been reasonable to expect that separation between OL and SL would have produced a much higher stress at the top fiber of OL than that predicted by ILLI-SLAB, because OL would be essentially responding as an unsupported cantilever. The implications of the closeness of the results from the two codes are therefore worth examining in some more detail. In the process it becomes apparent that correct interpretation of pavement behavior may often require consideration of the distributions of stresses and deflections instead of mere identification of maximum responses. For airport pavements in particular it is pertinent to recall that the estimation of the pass-to-coverage ratio for various aircraft may require the entire stress profile, not merely the maximum stress value. The

finite-element method is well-suited for response distribution determination.

For the aforementioned corner loading case, Figure 2 presents deflection profiles for SL and OL, obtained by using ILSL2 and ILLI-SLAB, along the edge at which the two B-727 tire prints were applied. Because it allows no separation the latter code shows that the more flexible OL follows the deflection profile of the stiffer SL. All three deflection profiles shown are practically coincident in the neighborhood of the loaded corner. ILSL2 predicts deflections of OL and SL within 2 percent of those from ILLI-SLAB for about 1.2 m (4 ft) from the loaded corner. This can be explained by the observation that the heavy applied load enforces contact between OL and SL in this region. Furthermore, the interlayer spring stiffness k_i is much higher than the subgrade modulus k, thereby contributing little to total OL deflection. Nevertheless, OL and SL deflection profiles from ILSL2 become significantly different at greater offsets from the loaded corner, where the effects of curling and separation become predominant. In this region ILSL2 predicts separation between OL and SL, allowing the unloaded OL corner to curl upward in response to the imposed negative g_{OL}. It is apparent that the ILLI-SLAB deflection profile for OL in this region is unrealistic. The deflection profile of the stiffer SL, on the other hand, remains practically unaffected by separation and is close to the corresponding profile obtained by using ILLI-SLAB.

Figure 3 presents a similar comparison of OL bending stresses for the same corner loading case. Both ILLI-SLAB and ILSL2 predict stress distributions of similar shape, if not of similar magnitude. To interpret these trends it may be recalled that according to Westergaard's theory a maximum tensile stress may be expected at about 1.8 m (6 ft) from the loaded corner (*12*). In this case, however, the second heavy tire print in ILSL2 causes a localized stress reversal, in a manner characteristic of edge loads, before the stress attains the expected maximum. This stress reversal is considerably more pronounced when compressibility effects are taken into account. It appears that, because of their respective assumptions, ILLI-SLAB treats the second tire print as a corner load, causing a much milder stress reversal.

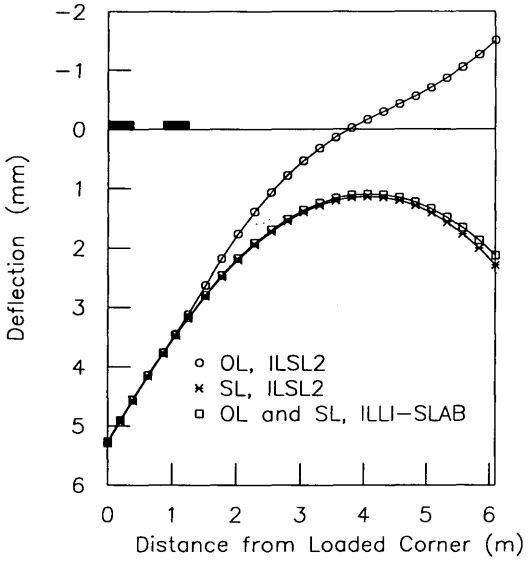

FIGURE 2 Deflection profiles from ILLI-SLAB and ILSL2 under corner loading and curling.

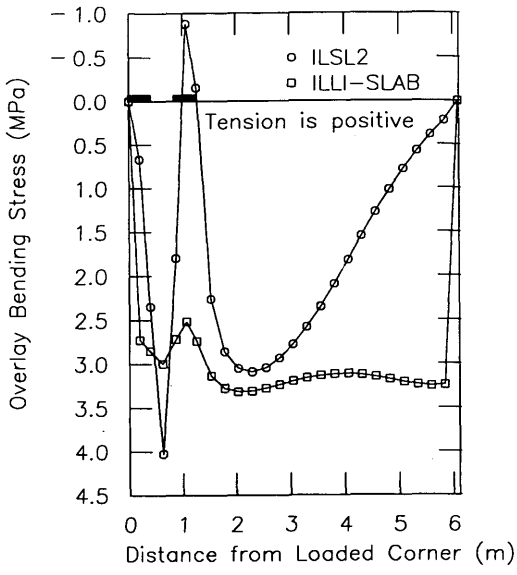

FIGURE 3 Overlay bending stress profiles from ILLI-SLAB and ILSL2 under corner loading and curling.

Interestingly, ILSL2 predicts that at greater offsets the tensile stress in OL decreases rapidly and smoothly to zero at the unloaded corner. For its part ILLI-SLAB suggests that OL stresses remain uniformly high until they are forced to return to zero by the boundary condition imposed at the unloaded corner. The higher stress level predicted by ILLI-SLAB for offsets greater than 2.5 m (100 in.) is attributable to the requirement that the OL follow the deflected shape of SL. The abrupt discontinuity observed in this case is evidence of the shortcomings of the conventional approach in ILLI-SLAB. It can therefore be concluded that agreement between the two codes with respect to maximum responses does not guarantee that response profiles predicted by each will be similar.

CONCLUSIONS

The study described here was undertaken in the context of a broader investigation into the behavior of multilayered concrete pavements. The specific objective was to develop a mechanistic tool for analysis of PCC pavements incorporating an unbonded PCC overlay and to use this in assessing the practical significance of the effects of layer compressibility and separation, as are likely to arise under conditions of dissimilar temperature gradients acting through the thicknesses of the existing slab and overlay.

The product of the study is a finite-element code, abbreviated herein as ILSL2, which represents an extension of the ILLI-SLAB program (1989 version). Numerous ILSL2 runs have been conducted for the purpose of verifying the new code. Practical illustrative examples pertaining to typical pavements are presented, and where appropriate these results are compared with existing analytical or numerical solutions, including those obtained by using ILLI-SLAB. It is found that both layer compressibility and separation effects need to be accommodated in a reliable mecha-

nistic model for unbonded PCC overlays. Although ILLI-SLAB often predicts maximum tensile stresses close to those predicted by ILSL2, stress and deflection profiles produced by the latter are more representative of actual pavement behavior. Furthermore, the conventional approach represented by ILLI-SLAB may sometimes underestimate significantly the maximum tensile stresses in the unbonded overlay in comparison with those estimated by ILSL2.

It has been found that combinations of temperature gradients through the slab and overlay having opposite signs are most detrimental to the pavement. When a heavy edge load is applied a positive temperautre gradient through the overlay and a negative gradient through the existing slab define the critical conditions for the existing slab; a negative gradient through the overlay acting together with a positive gradient through the existing slab is critical for the overlay. Under corner loading conditions, undesirable combinations of temperature gradients may create more critical conditions in the overlay than edge loading does. Therefore, ILSL2 can be especially helpful in assessing the potential for corner failures.

An unbonded overlay often contributes little to the flexural stiffness of the existing slab. Its beneficial effect on the performance of the pavement, however, is shown to be the result of thermal protection provided to the underlying slab. In addition, results obtained suggest that the overlay itself may be called on to carry a significant level of stress under certain severe combinations of temperature and external loadings. In fact even relatively thin overlays may experience tensile stresses higher than those developing in the existing slab. In contrast, conventional analysis, which ignores layer compressibility and separation effects, predicts lower stresses in the overlay if its flexural stiffness is lower than that of the existing slab. As a result the possibility of underdesigning unbonded PCC overlays is an issue that deserves serious reconsideration in conventional design approaches.

ACKNOWLEDGMENTS

This study was funded by the University of Illinois Campus Research Board (Grant 1-2-68437). The comments and suggestions of Arthur R. Robinson and Rami M. Hajali are greatly appreciated.

REFERENCES

1. Ioannides, A. M., L. Khazanovich, and J. L. Becque. Structural Evaluation of Base Layers in Concrete Pavement Systems. In *Transportation Research Record 1370*, TRB, National Research Council, Washington, D.C., 1992, pp. 20–28.
2. Van Dam, T., E. Blackmon, and M. Y. Shahin. Effect of Overlay Debonding on Pavement Performance. In *Transportation Research Record 1136*, TRB, National Research Council, Washington, D.C., 1987, pp. 119–132.
3. Hall, K. T., M. I. Darter, and W. J. Seiler. Improved Design of Unbonded Concrete Overlays. *Proc., 5th International Conference on Concrete Pavement Design and Rehabilitation*, Vol. 2, Purdue University, West Lafayette, Ind., April 20–22, 1993, pp. 227–240.
4. Totsky, O. N. Behavior of Multi-Layered Plates and Beams on Winkler Foundation (in Russian). *Stroitel'naya Mekhanika i Raschet Sooruzhenii*, No. 6, Moscow, 1981, pp. 54–58.
5. Korovesis, G. T. *Analysis of Slab-on-Grade Pavement Systems Subjected to Wheel and Temperature Loadings*. Ph.D. thesis. University of Illinois, Urbana, 1990.
6. Przemieniecki, J. S. Theory of Matrix Structural Analysis. McGraw-Hill, New York, 1968.
7. Khazanovich, L. *Structural Analysis of Multi-Layered Concrete Pavement Systems*. Ph.D. thesis. University of Illinois, Urbana, 1994.
8. Westergaard, H. M. New Formulas for Stresses in Concrete Pavements of Airfields. *Transactions, ASCE*, Vol. 113, 1948, pp. 425–439.
9. Mirambell, E. Temperature and Stress Distributions in Plain Concrete Pavements Under Thermal and Mechanical Loads. *Proc., 2nd International Workshop on the Design and Rehabilitation of Concrete Pavements*, Sigüenza, Spain, Oct. 1990, pp. 121–135.
10. Choubane, B., and M. Tia. Nonlinear Temperature Gradient Effect on Maximum Warping Stresses in Rigid Pavements. In *Transportation Research Record 1370*, TRB, National Research Council, Washington, D.C., 1992, pp. 11–19.
11. Tayabji, S. D., and P. A. Okamoto. Thickness Design of Concrete Resurfacing. *Proc., 3rd International Conference on Concrete Pavement Design and Rehabilitation*, Purdue University, West Lafayette, Ind., April 23–25, 1985, pp. 367–379.
12. Ioannides, A. M., M. R. Thompson, and E. J. Barenberg. Westergaard Solutions Reconsidered. In *Transportation Research Record 1043*, TRB, National Research Council, Washington, D.C., 1985, pp. 13–23.

Publication of this paper sponsored by Committee on Pavement Rehabilitation.